The Bacteriophage ϕ29 Head-Tail Connector Shows 13-Fold Symmetry in Both Hexagonally Packed Arrays and as Single Particles

Vladimir Tsuprun,* Dwight Anderson,‡ and Edward H. Egelman*
*Department of Cell Biology and Neuroanatomy and ‡Departments of Microbiology and Oral Science, University of Minnesota Medical School, Minneapolis, Minnesota 55455-0303 USA

ABSTRACT The symmetry of the ϕ29 head-tail connector is controversial: several studies of two-dimensional arrays of the connector have found a 12-fold symmetry, while a recent study of isolated particles has found a 13-fold symmetry. To investigate whether a polymorphism of the structure might explain these different results, electron microscopy and image analysis were used to study both isolated connectors and particles in hexagonally packed arrays. The hexagonally packed arrays have a P1 symmetry, and the connectors displayed 13 subunits both in the arrays and as isolated single particles. While we do not observe a polymorphism between connectors in two-dimensional arrays and as isolated particles, data show that the connectors can exist with either 12 or 13 subunits. A three-dimensional reconstruction of our 13-fold connector was generated by combining an averaged side-view projection with the known symmetry. The structure of rosettes of the connectors formed in the presence of ϕ29 prohead RNA (pRNA) was also examined. These rosettes contain five connectors arranged about a single connector in the center, and this arrangement may reflect an essential role of the pRNA in mediating a symmetry mismatch between either a 12- or 13-fold symmetric connector and a putative fivefold symmetric prohead portal vertex into which the connector fits.

INTRODUCTION

All tailed, double-stranded DNA bacteriophages contain a multimeric head-tail connector, located between the head and the tail, that functions in prohead assembly and DNA packaging (Bazinet and King, 1985; Casjens and Hendrix, 1988). Supercoiled DNA is wrapped around the bacteriophage ϕ29 connector in a nucleosome-like manner, suggesting that the packaging of DNA into the phage prohead initiates and proceeds by such a wrapping mechanism (Turnquist et al., 1992). Electron microscopy and image analysis have been used to study the structure of purified connectors from bacteriophages T3, T4, T7, λ, P22, SPP1, and ϕ29. Until recently, all connectors were described as having a 12-fold symmetry: T4 (Driedonks et al., 1981); λ (Kochan et al., 1984); T3 (Donate et al., 1988; Carazo et al., 1986b; Carrascosa et al., 1990; Valpuesta et al., 1992); P22 (Bazinet et al., 1988), and ϕ29 (Carrascosa et al., 1982, 1983, 1985; Carazo et al., 1984, 1985, 1986a; Jimenez et al., 1986). The bacteriophage SPP1 connector has now been studied and found to have a 13-fold symmetry (Dube et al., 1993), and these same authors have found a 13-fold symmetry for the ϕ29 connector and a 12-fold symmetry for the T4 connector. Kocsis et al. (1993a, 1993b) have found both a 12-fold and a 13-fold symmetry for the bacteriophage T7 connector.

Thus, the structure of the ϕ29 connector is controversial. Earlier analysis of the ϕ29 connector, with the finding of a 12-fold symmetry, was from hexagonally packed two-dimensional crystals (Carrascosa et al., 1982, 1983; Carazo et al., 1984, 1985; Jimenez et al., 1986) and tetragonally packed crystals (Carazo et al., 1986a), while recent analysis of isolated single particles found a 13-fold symmetry (Dube et al., 1993). However, a different analysis of isolated ϕ29 connectors found a 12-fold symmetry (Carrascosa et al., 1992). We have tested one possibility for the polymorphism of these structures: connectors with 12 subunits might pack preferentially into tetragonal or hexagonal arrays, while connectors with 13 subunits might be found preferentially as isolated particles. This would be consistent with the observations of Kocsis et al. (1993b), who found only a 12-fold symmetry for the T7 connector packed in hexagonal arrays, and both 12- and 13-fold symmetry for isolated T7 connectors. Therefore, hexagonally packed arrays as well as isolated single connectors overproduced and assembled from the ϕ29 gene 10 product (gp10) in *Escherichia coli* were examined.

MATERIALS AND METHODS

Protein preparation

gp10 of bacteriophage ϕ29 was purified from an overproducing *E. coli* strain as described (Garcia et al., 1984; Ibanez et al., 1984; Turnquist et al., 1992). For single particle preparations, the protein was diluted in a 50 mM Tris, 5% glycerol buffer (pH 7.7) to a final concentration of about 0.1 mg/ml and applied to glow-discharged carbon-coated grids. The samples were then negatively stained with 1% (w/v) uranyl acetate. Hexagonally packed two-dimensional arrays of the connector were formed by mixing protein samples diluted in the Tris-glycerol buffer to 0.1–0.5 mg/ml with an equal quantity of 5% (w/v) ammonium molybdate. This mixture was applied to the glow-discharged carbon-coated grids, and the excess was blotted with filter paper. The remaining thin film was allowed to air-dry for several minutes, resulting in the formation of the ammonium molybdate-stained hexagonal arrays. The

Received for publication 2 February 1994 and in revised form 23 March 1994.

Address reprint requests to Edward H. Egelman, Department of Cell Biology and Neuroanatomy, 4-135 Jackson Hall, University of Minnesota Medical School, 321 Church Street SE, Minneapolis, MN 55455-0303. Tel.: 612-626-0100; Fax: 612-624-8118; E-mail: egelman@egel1.med.umn.edu.

Abbreviation used: pRNA, prohead RNA.

0006-3495/94/06/2139/12 $2.00

rosette-like structures composed of six connectors were formed after mixing 6.4 ng of purified connector protein in a 89 mM Tris, 89 mM boric acid, 2.5 mM EDTA buffer (pH 8.0) with 0.9 ng of prohead RNA (pRNA), produced and purified as described (Wichitwechkarn et al., 1992).

Electron microscopy and image analysis

A JEOL 1200EXII electron microscope was used at an accelerating voltage of 80 kV and a magnification of 50,000×. Minimal dose procedures were used, such that specimens received no irradiation at high magnification before the recording of images on film. Electron micrographs were scanned with an Eikonik 78/99 digital camera interfaced to a VAX 3200 computer, resulting in a sampling of 3.6 Å/pixel. The SPIDER software system (Frank et al., 1981) was used for much of the image processing. Correspondence analysis (van Heel and Frank, 1981) was implemented within SPIDER.

Rotational power spectra (Crowther and Amos, 1971) were computed by first converting the Cartesian density distributions, $\rho(x,y)$, to cylindrical coordinates, $\rho(r,\theta)$, and then computing the integral:

$$g_n(r) = \int \rho(r,\theta) e^{in\theta}\, d\theta \qquad (1)$$

The rotational power, p_n, was then taken as:

$$p_n = \int |g_n(r)|^2\, r dr$$

Three-dimensional surfaces were generated with a Marching Cubes algorithm (Lorensen and Cline, 1987) and rendered with the Advanced Visualizer software (Wavefront Technologies) running on a Silicon Graphics Crimson Extreme workstation.

RESULTS

Isolated single particles

Two distinct forms of projections of the connector assembly were observed in images of negatively stained samples. The first type, a top view, was approximately circular with a diameter of 140–150 Å and had a stain-filled hole in the center (Fig. 1 *A*). The second type, a side view, appeared as an arrowhead, with a length of about 85 Å and a width of about 145 Å (Fig. 3 *A*). The side view displayed a prominent stain-filled central channel, and particles seen in this side view frequently aggregated into dimers or linear arrays, with all arrowheads oriented in the same direction (Fig. 3 *A*). Because of the poor signal/noise ratio, the symmetry of individual particles was not determined with any reliability. The averaging of a large number of such images was thus essential to visualize objectively structural detail within the connector. It has been shown that the use of a reference particle or model for the alignment of a population can strongly bias the result of averaging (Boekema et al., 1986). Therefore, a reference-free alignment procedure (Penczek et al., 1992) implemented within the SPIDER software system (Frank et al., 1981) was used for the rotations and translations of individual connectors to bring them into alignment.

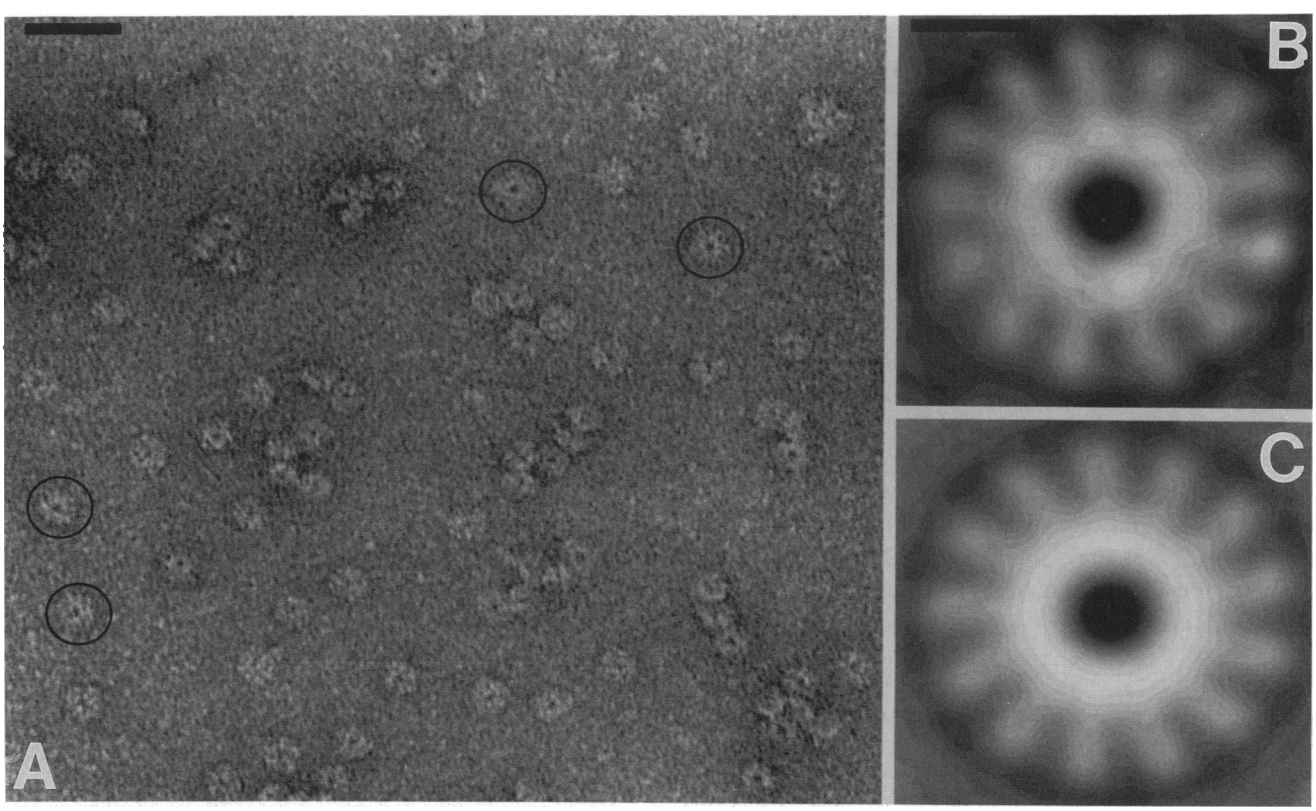

FIGURE 1 (*A*) A field of ϕ29 connectors (gp10 protein), negatively stained with uranyl acetate. The *circles* mark connectors that display the characteristic "top" view orientation, with the stain-filled central channel visible as a dark spot in the center. The scale bar is 400 Å. (*B*) An average image created from 81 individual connectors, after a reference-free translational and rotational alignment (Penczek et al., 1992) was performed on three subsets of the data. The subset averages were then aligned with the same algorithm to produce the average shown. (*C*) The average of *B*, after the imposition of 13-fold rotational symmetry. The scale bar in *B* is 50 Å.

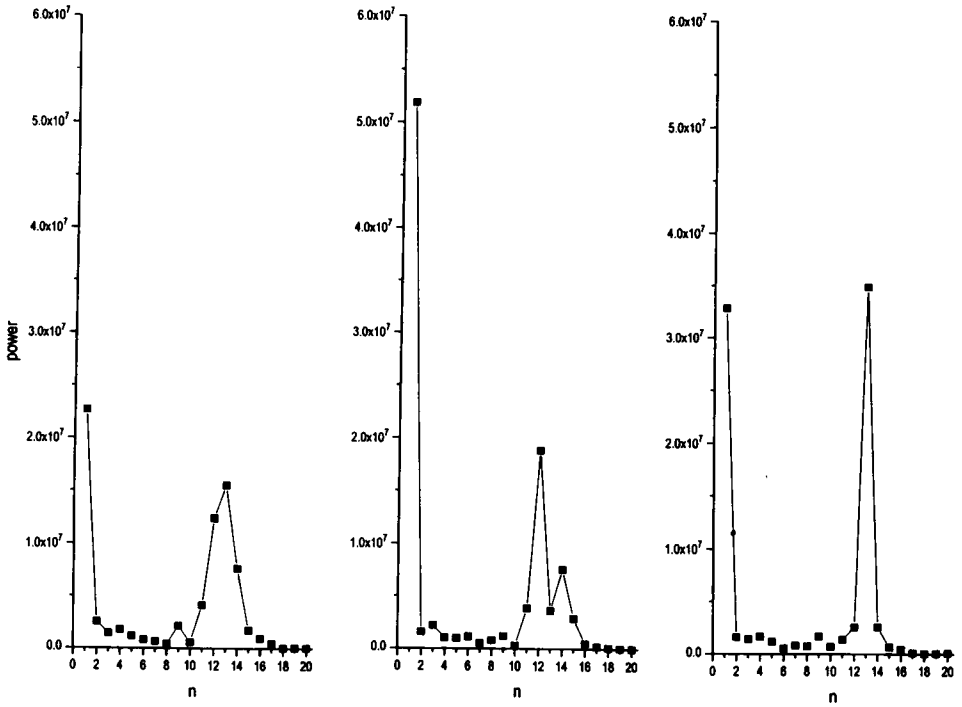

FIGURE 2 The rotational power spectrum of the average image, shown in Fig. 1 *B*, created from isolated single connectors. The power spectrum has been computed out to a radial limit of 90 Å. (*Left*) The rotational origin for the power spectrum has been taken as the center of mass of the image. (*Center*) The rotational origin has been chosen as the position that maximizes the 12-fold component. The shift of the origin from that in the *left* is 7.6 Å. (*Right*) The rotational origin has been taken as the position that maximizes the 13-fold component. The shift of the origin from that in the *left* is 6.5 Å, and the direction of the shift is approximately opposite to that in the *center*.

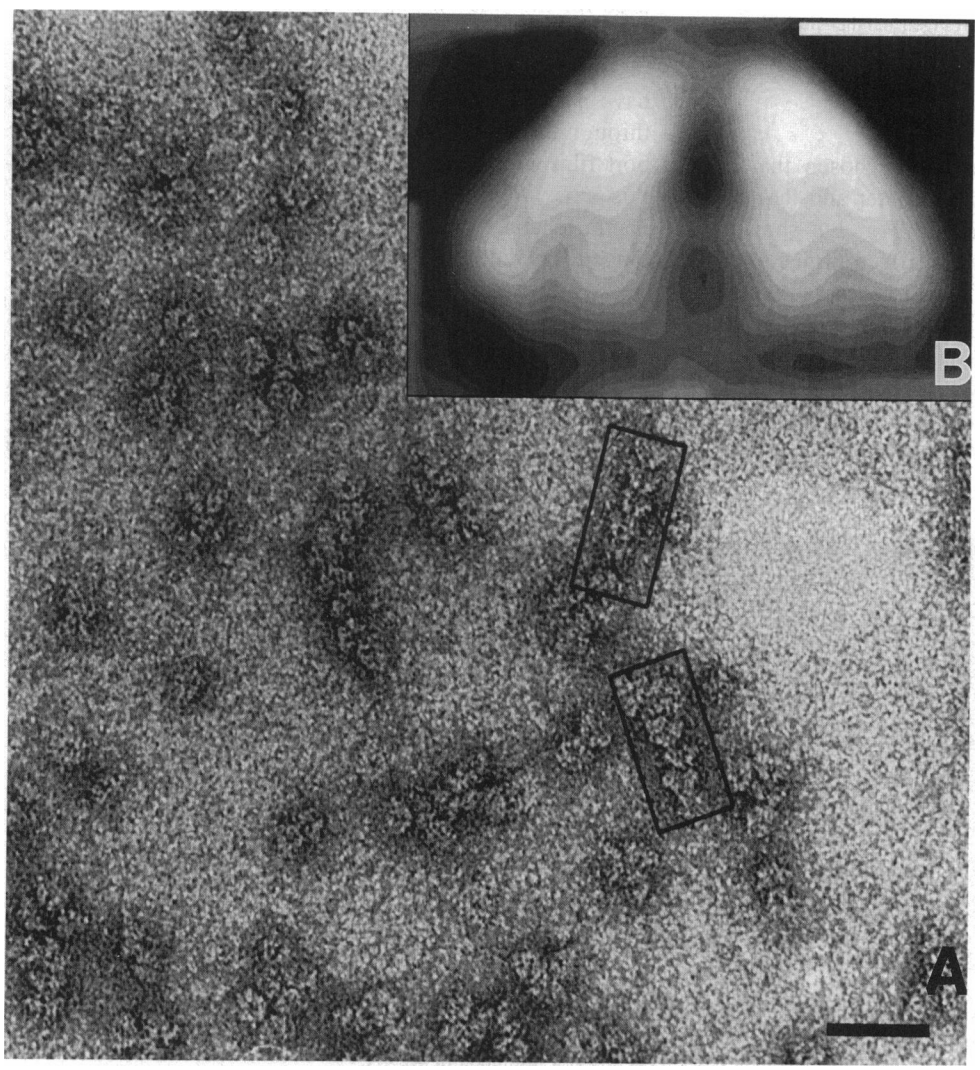

FIGURE 3 (*A*) A field of negatively stained ϕ29 connectors showing linear aggregates of the connectors in a "side"-view orientation (within rectangular boxes). The scale bar is 400 Å. (*B*) The average image of the side view, created from 211 individual images, after a reference-free rotational and translational alignment. The scale bar is 50 Å.

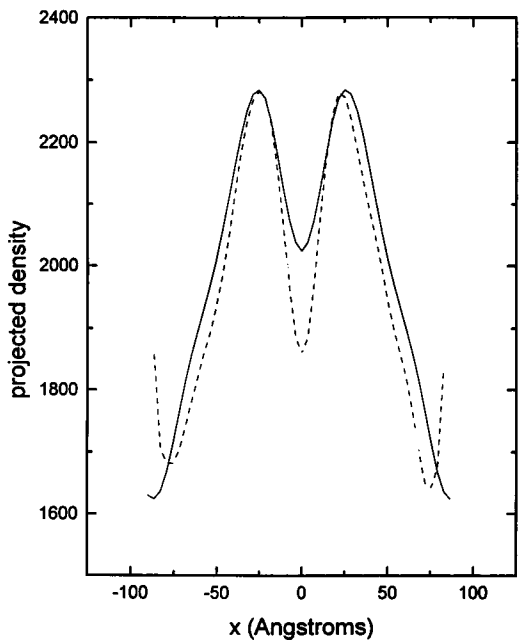

FIGURE 4 The averaged two-dimensional projections of the top view and the side view have been reduced to one-dimensional projections. The side view of Fig. 3 *B* has been projected onto the *x*-axis (*dashed line*), while the top view of Fig. 1 *B* has been cylindrically averaged and then projected onto the *x*-axis (*solid line*). The very good agreement shows that these two different projections (top and side) do arise from the same molecular structure.

Individual images of top views were chosen that displayed a clear stain-filled hole in the center and that were approximately cylindrically symmetric. Fig. 1 *B* shows an average of 81 individual top views. Thirteen projections in the image were clearly observed. Rotational power spectra of this average are shown in Fig. 2 for three different rotational origins, and it can be seen that the interpretation of such spectra can be misleading. While the image of Fig. 1 *B* clearly shows 13 subunits, in Fig. 2 *left* the rotational power spectrum, using the center of mass of the image as the origin of rotation, shows nearly equal power for the 12- and 13-fold rotational components. We interpret this as arising from noise, and it would not be expected to systematically bias the results of such rotational power searches in any one direction. Instead of fixing the rotational origin at the center of mass, when the origin of rotational symmetry was allowed to shift, the maximal rotational power is found for 13-fold symmetry, as shown in Fig. 2 *right*. When the rotational origin is shifted to maximize the 12-fold power (Fig. 2 *center*), the 12-fold power is less than the 13-fold power in Fig. 2 *right*. It can be seen that the $n = 1$ component increased when the rotational origin was shifted from the center of mass to the position that maximized the 13-fold component, suggesting that a density gradient across the average accounted for this shift between the two different rotational origins. A 13-fold symmetry was imposed upon the average of Fig. 1 *B* in Fig. 1 *C*. Because of the small number of particles used in this average, attempts to use correspondence analysis (van Heel and Frank, 1981) to decompose this average into subsets of images based upon similarity were not fruitful.

A similar procedure of reference-free alignment was used for the side views, except that images of the connectors in this view were taken from the linear arrays. It is reasonable to believe that the connectors in the arrays all have a common orientation of their central axis (running through the stain-filled channel) parallel to the carbon support film and that they may have variable rotations about this axis. After a selection based upon a clearly visible central channel, 220 side views of the connector were averaged together (Fig. 3 *B*). The assumption was made that the two different types of images (top and side views) correspond to orthogonal projections of the same object. This can be tested at this point, since the projection of the density of a three-dimensional object onto one dimension should be independent of the order in which the projections are taken. Thus, a projection of an arrowhead (side

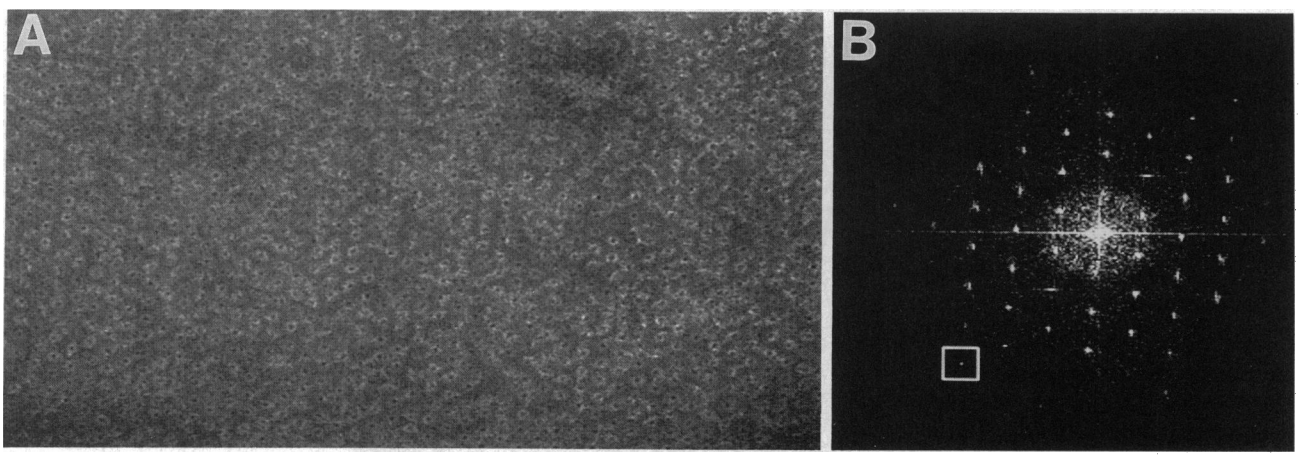

FIGURE 5 (*A*) Hexagonally packed two-dimensional array of the connector seen in the top view. The connectors have been negatively stained with ammonium molybdate. The mean center-to-center spacing of the connectors is 145 Å. (*B*) The computed Fourier transform intensities of an area about 3,150 Å × 3,150 Å, containing about 400 connectors. The *white box* indicates a reflection at a resolution of 1/29 Å.

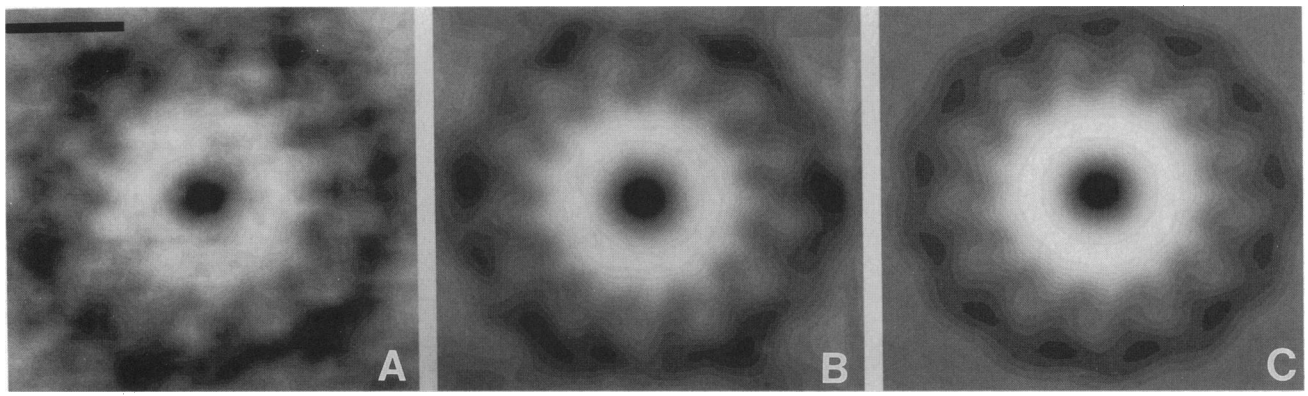

FIGURE 6 (*A*) An average of about 130 connectors from a single hexagonally packed crystalline patch. The average has been created using only translational averaging, with the translations determined from the cross-correlation function between the crystalline patch and a reference generated from averaging several connectors. The scale bar is 50 Å. The correlation averaging has been performed on 43 different crystalline patches. The resulting 43 averages have been aligned rotationally and translationally using the reference-free alignment, and the average of the 43 averages is shown in *B*. The average in *B*, containing about 5,500 individual connectors, has been 13-fold symmetrized in *C*.

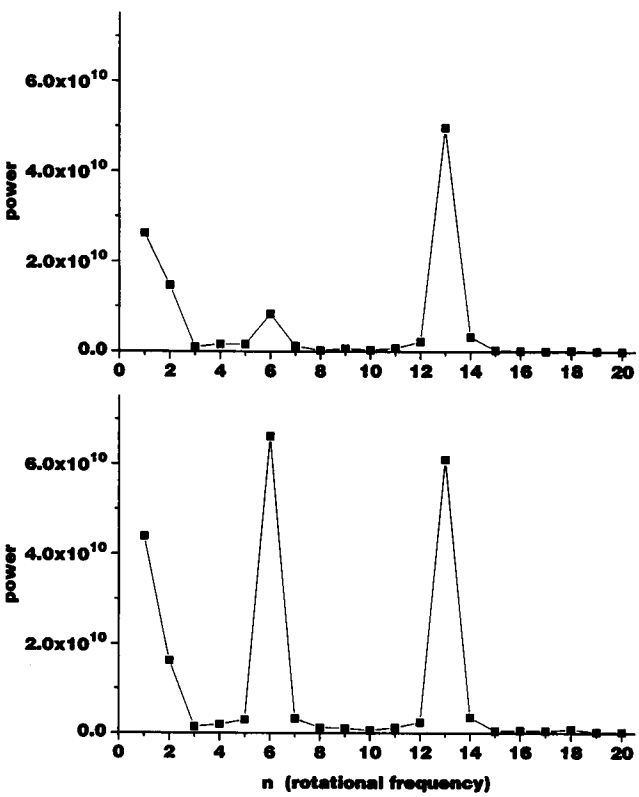

FIGURE 7 The rotational power spectrum of the average of Fig. 6 *B*, derived from hexagonally packed connectors. The power spectrum is shown with a 72 Å radial limit (*top*) and an 86 Å radial limit (*bottom*). The rotational origin for the power spectrum has been taken as the center-of-mass of the image.

view) onto the x-axis should be identical with the projection of the top view onto a particular tangential line. Because of the 13-fold symmetry displayed in the top view, there will be a range of $\pm 14°$ within which different projections of the top view may be generated. However, because the averaged side view in Fig. 3 *B* most likely represents the average of different rotational orientations about the central channel of the connector, the one-dimensional projection of the averaged side view of Fig. 3 *B* was compared with the one-dimensional projection of the top view of Fig. 1 *B* after cylindrical averaging. This comparison, shown in Fig. 4, suggests that the original assumption is quite legitimate, and the differences that do exist may be due to differences in staining between the two different orientations that arise as a result of their different relation to the carbon substrate.

Correlation-averaging of two-dimensional arrays

Fig. 5 *A* shows an example of a hexagonally packed array of the connectors. The computed Fourier transform of a region is shown in Fig. 5 *B*. The transform shows that the hexagonal lattice planes are spaced about 126 Å apart, and the center-to-center spacing of the connectors is therefore about 126 Å/(3/2), or 145 Å. Diffraction spots extend out to a resolution of about 1/29 Å. Visual inspection of the arrays, as well as Fourier filtration, show that the large arrays are highly mosaicked. Therefore, small (512 × 512 pixel) coherent patches, containing about 130 connectors, were used for all subsequent analysis.

A reference image was created by averaging together several individual connectors. The cross-correlation map of the reference with the 512 × 512 pixel hexagonal array was computed, and individual connectors were masked out of the array into 50 × 50 pixel boxes (180 Å × 180 Å) using the positions of the cross-correlation peaks. The images of the masked connectors were then simply averaged. From each crystalline patch, an average image was thus created that represented only translational alignment of the unit cells, with no rotational shifts allowed. These operations were repeated for 43 different areas. Each individual average showed 13 projections, and almost all of these 43 different averages had the 13 projections emerging from the central annulus with a left-handed twist. A typical average is shown

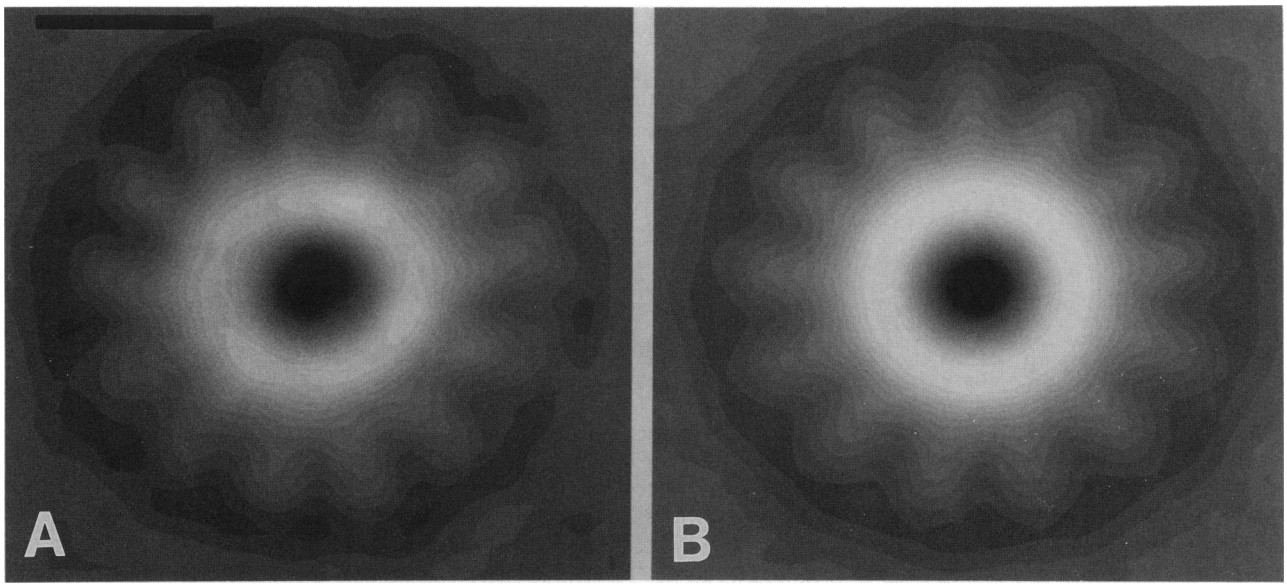

FIGURE 8 (*A*) An average of 81 connectors windowed out of the hexagonally packed arrays. The average has been generated using reference-free translational and rotational alignment of the individual connectors, first by creating averages of four subsets, and then averaging the subset averages using the same algorithm. The scale bar is 50 Å. (*B*) A 13-fold rotational symmetry has been imposed on the average of *A*.

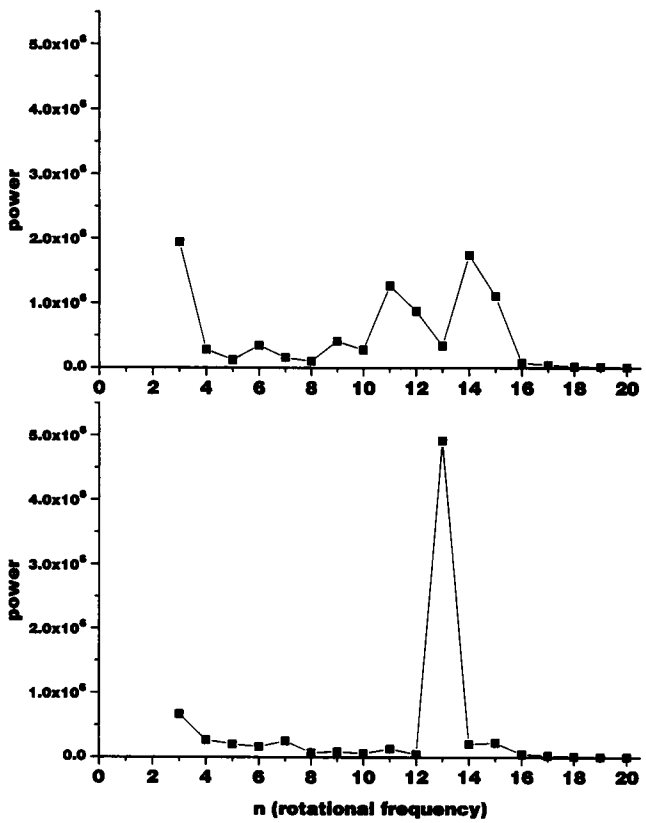

FIGURE 9 The rotational power spectrum of the average shown in Fig. 8. (*Top*) The rotational origin for the power spectrum has been taken as the center-of-mass of the image. (*Bottom*) The rotational origin has been taken as the position that yields the strongest 13-fold rotational power. The shift of the rotational origin between *A* and *B* is 10.9 Å, and the power spectra are dramatically different. Rotational orders 1 and 2 are not shown, since they dominate the power spectrum. The radial limit for the power spectra was 76 Å.

in Fig. 6 *A*. The 43 individual averages were then aligned translationally and rotationally using the reference-free alignment procedure (Penczek et al., 1992). The resulting average of the 43 subaverages is shown in Fig. 6 *B*. This average results from about 5,500 individual connectors and has had no symmetry imposed.

The difficulty in determining the symmetry within individual connectors might be expected to arise from a large flexibility of the structure. Therefore, the packing of the connectors into hexagonal or tetragonal arrays might be expected to perturb the symmetry of the structure, in a manner similar to that described for GroEL by Zahn et al. (1993). Surprisingly, the rotational power spectrum of the grand average of Fig. 6 *B*, computed within a radial limit of 72 Å (Fig. 7 *top*), shows only a weak sixfold component that is presumably due to the hexagonally packed environment of the individual connectors. When the radial limit is taken as 86 Å, the rotational power spectrum of Fig. 7 *bottom* shows the strong sixfold component that arises from the molecular packing. The clear 13-fold symmetry present in the averages of Fig. 6, *A* and *B*, and the power spectra of Fig. 7, provide the justification for the 13-fold symmetrized average shown in Fig. 6 *C*.

Single particle averaging from two-dimensional arrays

As an independent check on the translational alignment of connectors within the hexagonal crystals, individual connectors within these same arrays were masked and the reference-free alignment was used to rotationally and translationally orient the images of the single connectors. Connectors that displayed an even staining were cut out into 50 × 50 pixel boxes (180 Å × 180 Å), and the contribution of neighboring

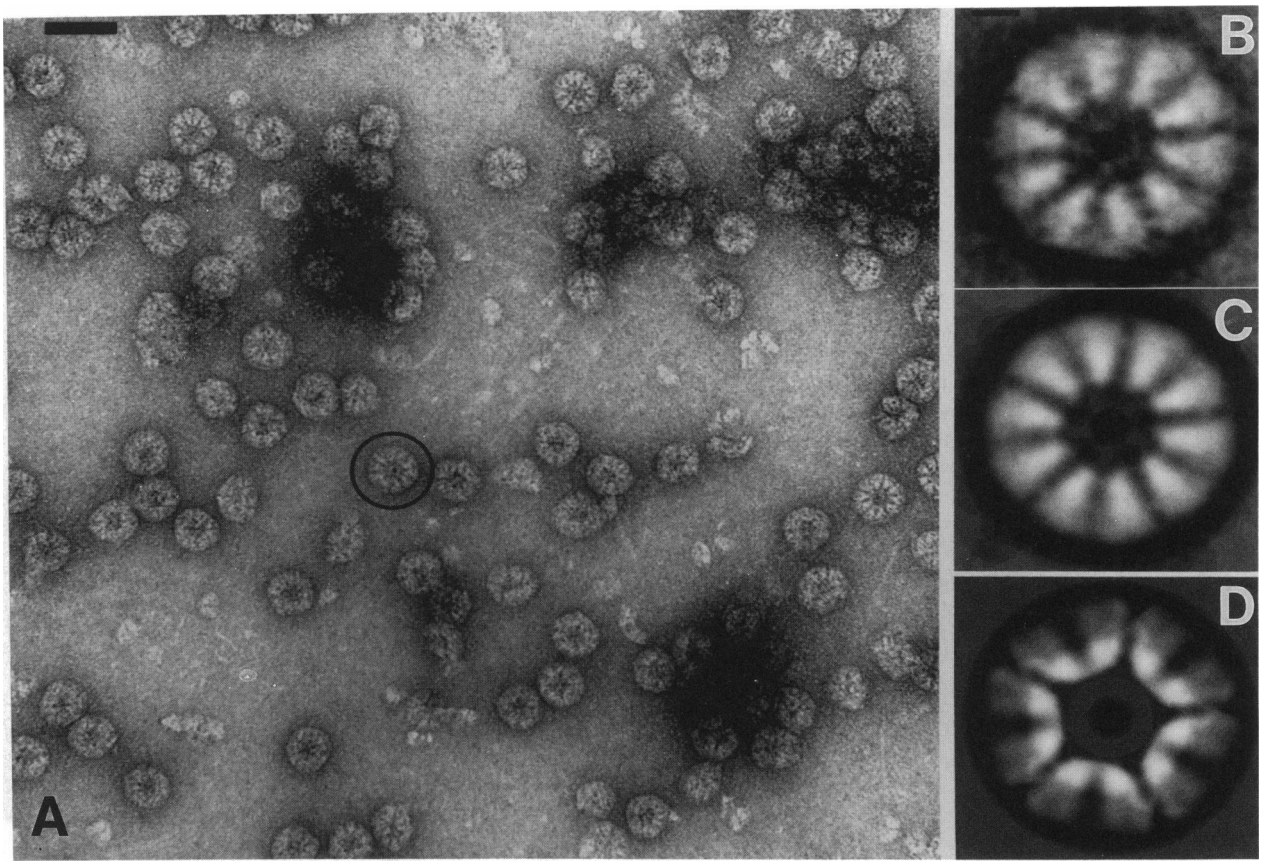

FIGURE 10 (*A*) A field of rosette-like particles, negatively stained with uranyl acetate. These rosettes are created when prohead RNA is added to the gp10 connector protein. The *black circle* marks a rosette, which displays the characteristic 35 Å diameter stain-filled central hole seen in the connector top views. This suggests that the centers of these rosettes contain a connector oriented in the top view. The scale bar is 600 Å. (*B*) An average of 60 of the rosettes, generated with the reference-free translational and rotational alignment of the individual rosettes. The average shows that there are five connectors, oriented in the side view, arranged about the central core. The rosette is approximately 400 Å in diameter, and the scale bar is 70 Å. (*C*) The average in *B* has been fivefold symmetrized. (*D*) A model rosette, created by using the averaged top view of Fig. 6 *C* in the center, surrounded by five averaged side views of Fig. 3 *B*.

connectors was minimized by imposing a circular mask with a radius of 23 pixels (83 Å) on each such box. Coincidentally, 81 connectors were used for this procedure (the same number as used for the single particle averaging of Fig. 1 *B*). The resulting average of these 81 connectors is shown in Fig. 8 *A*. The rotational power spectrum of this average is shown in Fig. 9 for two different rotational origins. The extreme sensitivity of the rotational power spectrum to the choice of origin, discussed in Crowther and Amos (1971), is illustrated in this figure. When the rotational origin is taken as the center of mass (Fig. 9 *top*), the 13-fold power is actually at a minimum near zero. However, when the origin is allowed to shift to maximize the 13-fold power (Fig. 9 *bottom*), the 13-fold power is clearly dominant. Although these connectors have been cut out of the hexagonal arrays, there is much less sixfold component in the power than in the corresponding connectors correlation-averaged from the arrays (Fig. 7). This difference is almost certainly due to the imposition of the mask, which will tend to nearly eliminate the contribution of the six nearest neighbors to the individual particles. A 13-fold symmetrized average is shown in Fig. 8 *B*.

Image analysis of rosette-like particles

In the presence of pRNA, ϕ29 connectors formed rosette-like particles, approximately 400 Å in diameter, that are shown in Fig. 10 *A*. These particles were formed in abundance in the presence of the pRNA and have also been observed with ribosomal 5 S RNA (data not shown), but were never seen in the absence of RNA. The centers of some of these particles (*black circle* in Fig. 10 *A*) show the approximately 35 Å diameter stain-filled hole that can be seen in top views of individual connectors (Fig. 1), suggesting that a single connector lies at the center of these particles. The reference-free translational and rotational alignment of 60 of these particles is shown in Fig. 10 *B*. This average displays a very striking 10-fold rotational periodicity. However, a comparison with the averaged side view of Fig. 3 *B* suggests that there are actually five connectors, oriented in a side view, around the center of this structure. The stain-filled central channel of the connectors thus generates the 10-fold periodicity from the five connectors. We have therefore imposed a fivefold averaging on Fig. 10 *B* to generate Fig. 10 *C*.

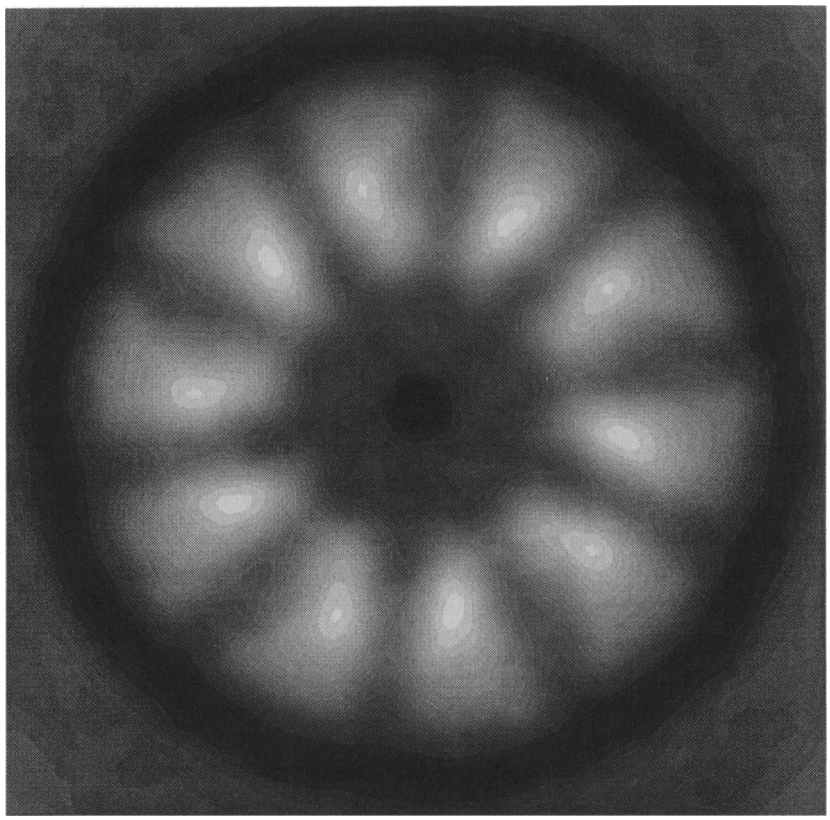

FIGURE 11 A fivefold rotational symmetry was imposed upon each of 60 individual rosettes, and the symmetrized images were then aligned using the reference-free algorithm. The resulting average shows a stronger fivefold periodicity than the average of Fig. 10 *C*, in which a fivefold symmetry has been imposed upon an average of unsymmetrized rosettes.

Support for this concept of the rosettes is given in Fig. 10 *D*, where we have assembled a model rosette by placing five copies of the averaged side view (Fig. 3 *B*) around a single copy of the averaged top view (Fig. 6 *C*). The central connector is not visible in the average of Fig. 10 *B*, since the alignment of the individual rosettes has been dominated by the fivefold and 10-fold periodicity of the surrounding connectors. Thus, a 13-fold symmetric density within the center will be averaged out. It can be seen that the five surrounding connectors overlap the central connector, giving rise to the increased density in the overlap region seen in the model of Fig. 10 *D* around the periphery of the central connector. The pseudo 10-fold symmetry of the model in Fig. 10 *D* suggests that the approximate 5-fold symmetry (approximate since the central connector does not have fivefold symmetry) may be weakened during the process of rotational alignment by misalignments of 360°/10 or 36°.

An improved average may therefore be generated by using prior knowledge of the structure. We have taken 60 images of the rosettes and imposed a fivefold symmetry on the individual rosettes before averaging. Unfortunately, because of the poor signal/noise ratio in individual images, attempts to localize the best origin of rotational symmetry by either maximizing the fivefold power or searching for the center of mass in each of the 60 images did not yield good solutions. Therefore, the rosettes were centered by eye, a fivefold symmetry was imposed, and the reference-free alignment was run on the symmetrized images. The resulting average of symmetrized images is shown in Fig. 11, where it can be seen that the fivefold character is stronger than in the corresponding average of Fig. 10 *C*, where a fivefold symmetry has been imposed upon the average of unsymmetrized images. The average of Fig. 11 provides support for our assumption that there is a connector located at the center of the rosette. If the structure did not contain a central connector, the density in the center (up to 60 Å radius) should be uniform black, the same density as the ~35 Å diameter hole in the center or the stain surrounding the rosette. The density that is seen between 17 and 60 Å radius is consistent with that of a single connector.

The possible relationship between the pRNA and the fivefold environment of the central connector to the prohead-connector interface of the intact bacteriophage is discussed below.

Three-dimensional reconstruction of the connector

For an asymmetric object of diameter D, it is necessary to have $N = \pi D/d$ projections of the object, where these projections represent evenly spaced rotational views, in order to reconstruct the object to a resolution d (Crowther et al., 1970). Using the 13-fold symmetry, a single side view of the connector can thus be used to reconstruct the 145 Å diameter connector in three dimensions at a resolution of 35 Å. Correspondence analysis was used in an attempt to decompose the averaged side view of Fig. 3 *B* into discrete subsets (Fig. 12). Since the top view of the connector is known, it should

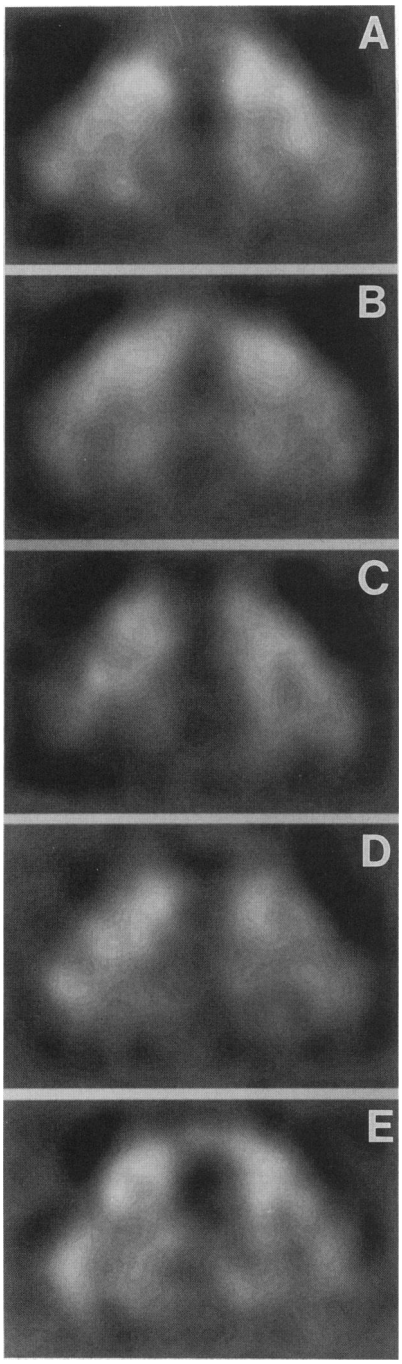

FIGURE 12 Correspondence analysis has been used to generate five subsets of the averaged side view of Fig. 3 *B*. The averages contained: (*A*) 43 images, (*B*) 49 images, (*C*) 31 images, (*D*) 27 images, and (*E*) 31 images.

be possible to find different characteristic side views that may be related to projections of the top view at different angles.

We have only found a single class of side views, that of Fig. 12 *A*, that can be used in a three-dimensional reconstruction, such that the "top view" projection of the resulting reconstruction agrees well with the independently determined averaged top view. Attempts to incorporate other side views in such a reconstruction gave rise to projections that were not simply related to our other data. Thus, the averaged subsets of Fig. 12, *B-E*, probably do not arise from simple axial rotations of the connector, but may represent off-axis tilts, stain anomalies, etc. We have therefore used only the single averaged view of Fig. 12 *A*, containing 43 images, combined with a 13-fold symmetry, to generate the reconstruction shown in Fig. 13. For purposes of comparison, we have chosen a surface threshold for the rendering that encloses a volume of 363,000 Å^3, which is the same enclosed volume shown by Carazo et al. (1986) for their ϕ29 connector reconstruction. This corresponds to about 66% of the expected molecular volume, and not 100% as stated in that paper. The structure appears as a nearly hemispherical shell, with an approximately 35 Å diameter hole at the pole, and 13 protruding subunits near the equator.

Two orthogonal projections of the three-dimensional reconstruction are shown in Fig. 14. Fig. 14 *A* provides a direct comparison with the top view of Fig. 1 *C*. It can be seen that in Fig. 1 *C* the radial density falls off nearly monotonically, while in the projection of Fig. 14 *A* the radial density rises to a peak around the central hole, falls, and then rises again. This is very similar to the top view projection of the ϕ29 connector shown by Dube et al. (1993). Although differences exist between the actual top view of Fig. 1 *C* and the simulated top view of Fig. 14 *A*, the general agreement is quite good and provides a justification for the reconstruction from the side view. Similarly, we have cylindrically averaged the three-dimensional reconstruction and generated a side view projection in Fig. 14 *B*. This can be compared with the averaged side view projection in Fig. 3 *B*. The agreement is good, but differences that do exist may be due to the fact that the averaged side view of Fig. 3 *B* does not actually represent cylindrically averaged density. That is, particular orientations (within a 28° rotational range) may be dominant in the real side views. However, the assumption that Fig. 3 *B* represents cylindrically averaged density did not enter into the reconstruction.

DISCUSSION

We have explored the possibility that a polymorphism in the ϕ29 connector structure might exist, such that isolated single particles display a 13-fold symmetry (Dube et al., 1993) while tetragonally packed (Carazo et al., 1986a) and hexagonally packed (Carrascosa et al., 1982, 1983; Carazo et al., 1984, 1985; Jimenez et al., 1986) connectors display a 12-fold symmetry. If such a polymorphism did exist, hexagonally packed arrays might be expected to have a P6 symmetry and contain 12-fold symmetric connectors. Surprisingly, our hexagonally packed arrays had a P1 symmetry, since pure translational averaging of the unit cells produced a well-defined connector image that appeared very similar to the single-particle averaged ϕ29 connector shown by Dube et al. (1993). Could the differences between observations of 12- and 13-fold symmetry be a result of image analysis methods?

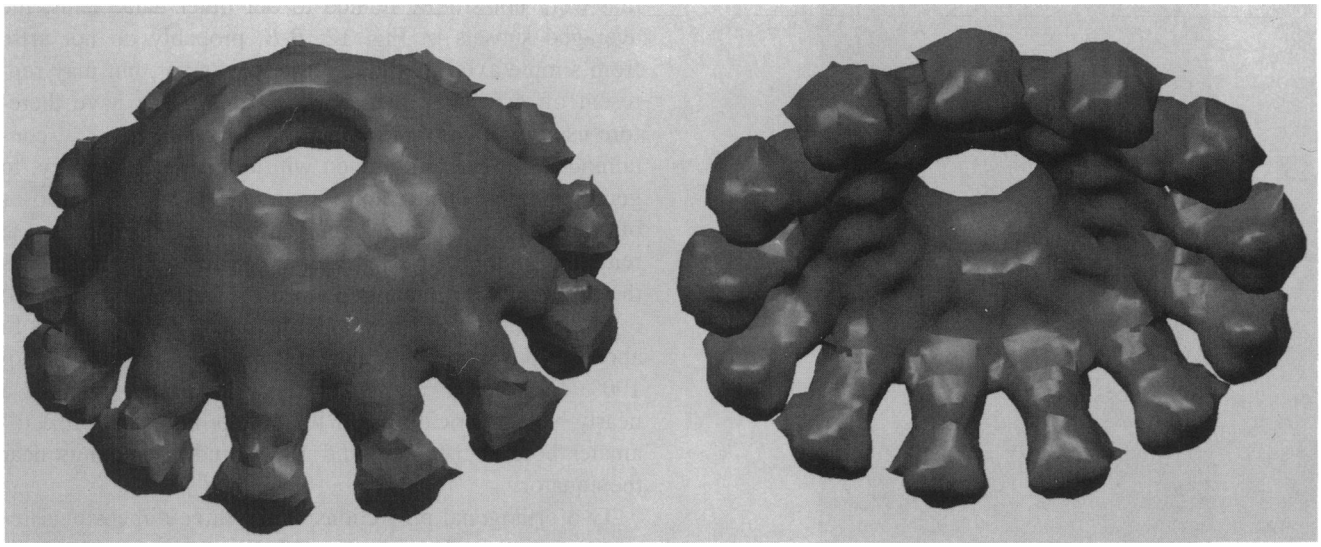

FIGURE 13 Two views of a three-dimensional reconstruction of the ϕ29 connector obtained by using the side view of Fig. 12 *A* combined with the 13-fold symmetry determined from the top views. The surface that is shown contains about 66% of the expected molecular volume.

We have obtained pictures of isolated ϕ29 connectors prepared, imaged, and selected by the Madrid group and analyzed these images by similar methods to those used here. The average had a clear 12-fold symmetry, while our selected images analyzed in Madrid showed a clear 13-fold symmetry (E. H. Egelman, V. Tsuprun, J. M.Carazo and J. L. Carrascosa, unpublished observations). However, we have been able to perform electron microscopy on a connector sample from Madrid and extract one subset of images that averages as 12-fold, and a second subset that averages as 13-fold. This suggests that the polymorphism does exist within a sample, is most likely not a function of the isolation, purification, and preparation for electron microscopy, and may be a function of the selection of images. The resolution of this question is beyond the scope of the present paper, but is being addressed.

Do our results exclude entirely a polymorphism within our samples in the number of subunits in the connector? The answer appears to be no, since a mixed population of 12- and 13-fold symmetric connectors could still average together into a 13-fold symmetric structure if there were a majority of 13-subunit connectors. Modeling studies (data not shown) suggested that an approximately equal mixture of 12- and 13-fold symmetric structures would not average together as the real data have. If there is a polymorphism in our selected connectors, the percentage of connectors with 12 subunits was estimated to be less than 25%, but this estimate from the modeling studies was based upon assumptions about the signal/noise ratio and other factors.

Could the observed polymorphism be the result of an artefact of negative stain preparation? This appears unlikely, as such an artefact would most likely affect isolated connectors. Two-dimensional crystals from Madrid contain connectors with 12 subunits, while the two-dimensional crystals that we have described here contain connectors with 13 subunits. Cryo-electron microscopy of unstained specimens would be a method of examining unstained, fully hydrated isolated connectors, but the very poor signal/noise ratio that would be present in the images would make this task formidable.

Since it is evident that a polymorphism in the structural symmetry does exist, it is interesting to note that our three-dimensional reconstruction from single particles, with 13 subunits (Fig. 13), does not compare well with that obtained by Carazo et al. (1986) from crystals, with 12 subunits. While their reconstruction appeared as a solid structure, with a flat solid base and a cylindrical hole running through the entire structure, our reconstruction appears more as a hemispherical shell with a hole in the center of this shell. However, when the bacteriophage ϕ29 neck complex, containing the gp11 protein in addition to the gp10 connector protein, was reconstructed from two-dimensional crystals (Donate et al., 1988), the reconstruction showed a hemispherical shell for the connector that was similar in appearance to that seen for our isolated connector. Thus, it is possible that the connector is not only polymorphic with respect to the number of subunits, but may adopt two different conformations: the open shell for the isolated particle, and for the connector-gp11 complex in crystals, and a closed form for the connector alone in crystals.

The RNA-induced rosettes of connectors provide an interesting vehicle for further study of the connectors. They provide an additional confirmation for the averaged side view of Fig. 3 *B*, since Fig. 10 *D* shows that a model rosette built from the averaged side view matches the averaged rosette structure quite well. More importantly, the rosettes show that in the presence of RNA the central connector adopts a fivefold symmetry with respect to the binding of the outer connectors. Biochemical data suggest that there are about 18 copies of the pRNA associated with each rosette (data not shown). If so, there may be three copies of the RNA associated with each connector. The significance of this is that pRNA is essential for DNA packaging into the prohead

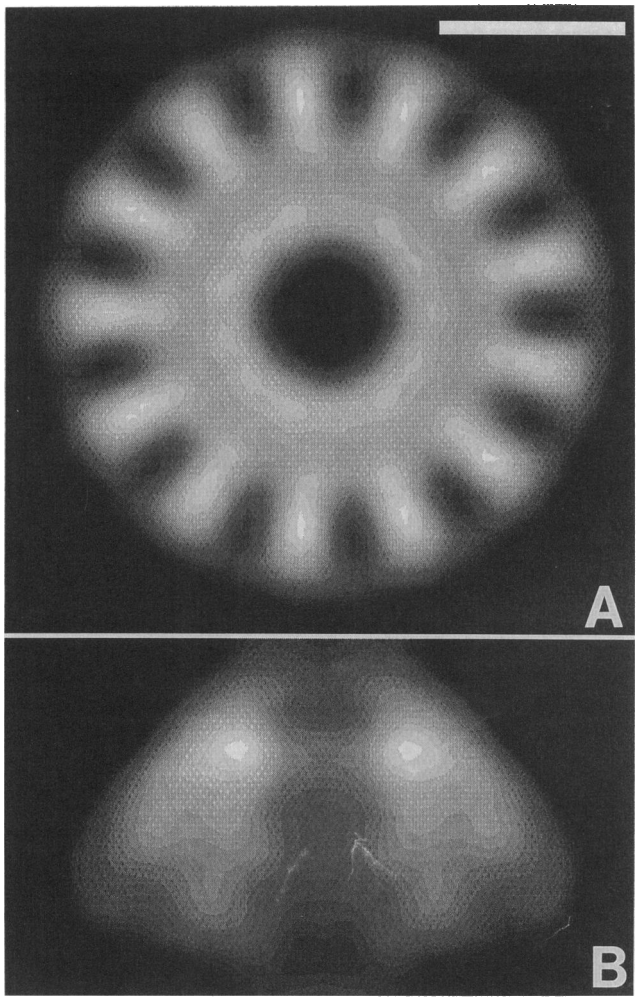

FIGURE 14 Two orthogonal projections of the density of the three-dimensional reconstruction of Fig. 13 onto a plane, generating a "top view" (*A*) and a cylindrically averaged "side view" (*B*). The scale bar is 50 Å. Although only data from a single side view were used in the reconstruction, the top view generated from these data compares quite well with the top view of Fig. 1 *C*. The cylindrically averaged side view projection compares quite well with the averaged side view of Fig. 3 *B*.

(Guo et al., 1987; Anderson and Bodley, 1990; Anderson and Reilly, 1993). It has also been suggested for phage P22 that protein-RNA interactions may be important in the assembly of the connector into the prohead (Bazinet et al., 1990). Alternatively, it may be possible that while the RNA induces a connector-connector aggregation, the arrangement of five connectors about the central connector may only be governed by steric constraints. That is, six or more connectors may not fit at the given radius of contact. The specificity for five outer connectors cannot be answered at this time.

All spherical viruses examined to date and the proheads of the phages P2 (Dokland et al., 1992), P4 (Dokland et al., 1992), P22 (Prasad et al., 1993), HK97 (Conway et al., 1993), and λ (Dokland and Murialdo, 1993) have icosahedral symmetry. While there is no direct evidence, it is widely believed that the connector particle replaces a fivefold symmetric vertex in the prohead. Thus, the connector forms a "portal vertex" that serves as core of the DNA packaging machine (Bazinet and King, 1985; Casjens and Hendrix, 1988). While the ϕ29 prohead, a prolate structure with a flattened base, cannot be icosahedral, the local packing of the shell may be nearly icosahedral. Thus, the rosettes may serve as a model for how the pRNA mediates a symmetry mismatch between either a 12- or 13-fold symmetric connector and a fivefold symmetric environment in which the connector sits. Clearly, more detailed information about the role of the pRNA in mediating this mismatch is needed.

This work was supported by National Institutes of Health Grants GM35269 (E. H. Egelman) and GM39931 and DE03606 (D. Anderson).

We would like to thank Drs. Pawel Penczek and Joachim Frank for assistance with the SPIDER software system and for helpful discussions and Sarah Turnquist for purifying the connectors and pRNA. We also thank Drs. Jose-Maria Carazo and Jose Carrascosa for freely sharing their data and protein preparations, as well as for helpful discussions.

REFERENCES

Anderson, D., and J. W. Bodley. 1990. Role of RNA in bacteriophage ϕ29 DNA packaging. *J. Struct. Biol.* 104:70–74.

Anderson, D. L., and B. E. Reilly. 1993. Morphogenesis of bacteriophage ϕ29. *In Bacillus subtilis* and Other Gram-Positive Bacteria: Physiology, Biochemistry and Molecular Genetics. J. A. Hoch, R. Losick, and A. L. Sonenshein, editors. ASM Publications, Washington, DC. 859–867.

Bazinet, C., J. Benbasat, J. King, J. M. Carazo, and J. L. Carrascosa. 1988. Purification and organization of the gene 1 portal protein required for phage P22 DNA packaging. *Biochemistry.* 27:1849–1856.

Bazinet, C., and J. King. 1985. The DNA translocating vertex of dsDNA bacteriophage. *Annu. Rev. Microbiol.* 39:109–130.

Bazinet, C., R. Villafane, and J. King. 1990. Novel second-site suppression of a cold-sensitive defect in phage P22 procapsid assembly. *J. Mol. Biol.* 216:701–716.

Boekema, E. J., J. A. Berden, and M. G. van Heel 1986. Structure of mitochondrial F_1-ATPase studied by electron microscopy and image processing. *Biochim. Biophys. Acta.* 851:353–360.

Carazo, J. M., L. E. Donate, L. Herranz, J. P. Secilla, and J. L. Carrascosa. 1986a. Three-dimensional reconstruction of the connector of bacteriophage ϕ29 at 1.8 nm resolution. *J. Mol. Biol.* 192, 853–867.

Carazo, J. M., H. Fujisawa, S. Nakasu, and J. L. Carrascosa. 1986b. Bacteriophage T3 gene 8 product oligomer structure. *J. Ultrastruct. Mol. Struct. Res.* 94:105–113.

Carazo, J. M., N. Garcia, A. Santisteban, and J. L. Carrascosa. 1984. Structural study of tetragonal-ordered aggregates of phage ϕ29 necks. *J. Ultrastruct. Res.* 89:79–88.

Carazo, J. M., A. Santisteban, and J. L. Carrascosa. 1985. Three-dimensional reconstruction of bacteriophage ϕ29 neck particles at 2.2 nm resolution. *J. Mol. Biol.* 183:79–88.

Carrascosa, J. L., J. M. Carazo, and N. Garcia. 1983. Structural localization of the proteins of the head to tail connecting region of bacteriophage ϕ29. *Virology.* 124:133–143.

Carrascosa, J. L., J. M. Carazo, C. Ibanez, and A. Santisteban. 1985. Structure of phage ϕ29 connector protein assembled in vivo. *Virology.* 141: 190–200.

Carrascosa, J. L., S. Marco, J. M. Valpuesta, L. E. Donate, and J. M. Carazo. 1992. Two-dimensional averaging of isolated phage ϕ29 connectors. *In* Electron Microscopy. Vol. 1. EUREM 92. 409–410.

Carrascosa, J. L., E. Vinuela, N. Garcia, and A. Santisteban. 1982. Structure of the head-tail connector of bacteriophage ϕ29. *J. Mol. Biol.* 154: 311–324.

Casjens, S., and R. Hendrix. 1988. The Bacteriophages, Vol. I. R. Calendar, editor. 15–91. Plenum Press, New York.

Conway, J. F., N. Cheng, R. L. Duda, R. W. Hendrix, and A. C. Steven. 1993. Structural changes along the capsid assembly pathway of bacteriophage

HK97. *The XIIIth Int. Conf. on Virus and Bacteriophage Assembly, Syria, VA.*

Crowther, R. A., and L. A. Amos. 1971. Harmonic analysis of electron microscopic images with rotational symmetry. *J. Mol. Biol.* 60:123–130.

Crowther, R. A., D. J. DeRosier, and A. Klug. 1970. The reconstruction of a three-dimensional structure from projections and its application to electron microscopy. *Proc. R. Soc. Lond.* A317:319–340.

Dokland, T., B. H. Lindquist, and S. D. Fuller. 1992. Image reconstruction from cryo-electron micrographs reveals the morphopoietic mechanism in the P2-P4 bacteriophage system. *EMBO J.* 11:839–846.

Dokland, T., and H. Murialdo. 1993. Structural transitions upon expansion of lambda heads. *The XIIIth Int. Conf. on Virus and Bacteriophage Assembly, Syria, VA.*

Donate, L. E., L. Herranz, J. P. Secilla, J. M. Carazo, H. Fujisawa, and J. L. Carrascosa. 1988. Bacteriophage T3 connector: three-dimensional structure and comparison with other viral head-tail connecting regions. *J. Mol. Biol.* 201:91–100.

Driedonks, R. A., A. Engel, B. tenHeggeler, and R. van Driel. 1981. Gene 20 product of bacteriophage T4. Its purification and structure. *J. Mol. Biol.* 152:641–662.

Dube, P., P. Tavares, R. Lurz, and M. van Heel. 1993. The portal protein of bacteriophage SPP1: a DNA pump with 13-fold symmetry. *EMBO J.* 12:1303–1309.

Frank, J., B. Shimkin, and H. Dowse. 1981. SPIDER—a modular software system for electron image processing. *Ultramicroscopy.* 6:343–358.

Garcia, J. A., E. Mendez, and M. Salas. 1984. Cloning, nucleotide sequence and high level expression of the gene coding for the connector protein of *Bacillus subtilis* phage ϕ29. *Gene.* 30:87–98.

Guo, P., S. Erickson, and D. L. Anderson. 1987. A small viral RNA is required for in vitro packaging of bacteriophage ϕ29 DNA. *Science (Wash. DC).* 236:690–694.

Ibanez, C., J. A. Garcia, J. L. Carrascosa, and M. Salas. 1984. Overproduction and purification of the connector protein of *Bacillus subtilis* phage. *Nucleic Acids. Res.* 12:2351–2365.

Jimenez, J., A. Santisteban, J. M. Carazo, and J. L. Carrascosa. 1986. Computer graphic display method for visualizing three-dimensional biological structures. *Science (Wash. DC).* 232:1113–1115.

Kochan, J., J. L. Carrascosa, and H. Murialdo. 1984. Bacteriophage lambda preconnectors. Purification and structure. *J. Mol. Biol.* 174:433–447.

Kocsis, E., M. E. Cerritelli, N. Cheng, B. L. Trus, and A. C. Steven. 1993a. Polymorphism of the head-to-tail connector complex of bacteriophage T7: 13-fold and 12-fold symmetric variants. *XIIIth Int. Conf. on Virus and Bacteriophage Assembly, Syria, VA.*

Kocsis, E., M. E. Cerritelli, B. L. Trus, and A. C. Steven. 1993b. Determination of rotational symmetry in macromolecules. *Biophys. J.* 64:64a (Abstr).

Lorensen, W. E., and H. E. Cline. 1987. Marching cubes: a high resolution 3D surface construction algorithm. *Comp. Graphics.* 21:163–169.

Penczek,, P., M. Radermacher, and J. Frank. 1992. Three-dimensional reconstruction of single particles embedded in ice. *Ultramicroscopy.* 40: 33–53.

Prasad, B. V., P. E. Prevelige, E. Marietta, R. O. Chen, D. Thomas, J. King, and W. Chiu 1993. Three-dimensional transformation of capsids associated with genome packaging in a bacterial virus. *J. Mol. Biol.* 231: 65–74.

Turnquist, S., M. Simon, E. Egelman, and D. Anderson. 1992. Supercoiled DNA wraps around the bacteriophage ϕ29 head-tail connector. *Proc. Natl. Acad. Sci. USA.* 89:10479–10483.

Valpuesta, J. M., H. Fujisawa, S. Marco, J. M. Carazo, and J. L. Carrascosa. 1992. Three-dimensional structure of T3 connector purified from overexpressing bacteria. *J. Mol. Biol.* 224:103–112.

van Heel, M., and J. Frank. 1981. Use of multivariate statistics in analyzing the images of biological macromolecules. *Ultramicroscopy.* 6:187–194.

Wichitwechkarn, J., D. Johnson, and D. L. Anderson. 1992. Mutant prohead RNAs in the in vitro packaging of bacteriophage ϕ29 DNA-gp3. *J. Mol. Biol.* 223:991–998.

Zahn, R., J. R. Harris, G. Pfeifer, A. Pluckthun, and W. Baumeister. 1993. Two-dimensional crystals of the molecular chaperone GroEL reveal structural plasticity. *J. Mol. Biol.* 229:579–584.